Supporting Information

Single-atomic Fe sites decorated N-doped carbon toward oxygen reduction in MFCs

Cui-e Zhao,[a] Wei Luo,[a] Haoran Tian,[a] Tao Lu,[a] Lei Yi,[a] Ying Zhang,[a] Li Shi*[a] and Yanwen Ma*[a, b]

[a]Key Laboratory for Organic Electronics and Information Displays & Jiangsu Key Laboratory for Biosensors, Institute of Advanced Materials (IAM), Jiangsu National Synergetic Innovation Center for Advanced Materials (SICAM), Nanjing University of Posts & Telecommunications, Nanjing 210023, China;

[b]Suzhou Vocational Institute of Industrial Technology, 1 Zhineng Avenue, Suzhou International Education Park, Suzhou 215104, China.

***Correspondences:** iamlshi@njupt.edu.cn;
iamywma@njupt.edu.cn

Experimental Details

Number of pages: 12

Number of figures: 12, Figures S1 to S12

Number of tables: 3, Tables S1 to S3

Experimental Details

1. Preparation of Fe-N-C.

The atomically dispersed Fe-N-C was derived from Fe-coordinated ZIF. Specifically, $Zn(NO_3)_2 \cdot 6H_2O$ (10 mmol) and $Fe(SO_4)_2 \cdot 7H_2O$ (from 0.1, 0.2, 0.3, 0.4 to 0.5 mmol) were first dissolved in 150 mL methanol and stirred thoroughly. Then, the mixtures were added to 2-methylimidazole (MeIm) solution (3.94 g in 150 mL methanol) under stirring and placed under 60 °C for 12 hours, respectively. Subsequently, Fe-coordinated ZIF with different Fe doping were obtained through varying initial amount of Fe salts in the precursor. After that, the light yellow powders were separated by centrifugation, followed by drying at 60°C. Finally, Fe-ZIFs were calcined under Ar flow at 900°C for 5 hours (3°C/min), and the Fe-N-C-X (X=0.1~0.5) were synthesized at high temperature. In addition, zeolitic imidazolate framework (ZIF-8) white powder was also fabricated by mixing MeIm and $Zn(NO_3)_2$ without Fe doping to derive the N-doped carbon (N-C).

2. Characterizations.

The morphology of Fe-N-C materials were acquired by using scanning electron microscopy (SEM, Hitachi S4800) and transmission Electron Microscopy (TEM, Hitachi HT7700). High-resolution TEM element mapping images and Ring-like selected area electron diffraction (SAED) were collected on a FEI G2F30 microscope. X-ray diffraction (XRD) spectra were analyzed on a Bruker D8 Advance A25. The surface element and chemical bond of Fe-N-C were performed using X-ray photoelectron spectroscopy (XPS, Kratos Axis Supra). The doped content of Fe in Fe-N-C-X samples were determined using Inductive coupling plasma mass-spectrometry (ICP-MS, NEXION 2000, PerkinElmer). The porous properties and Brunauer-Emmett-Teller (BET) specific surface area were probed by Nitrogen adsorption/desorption isotherm on an ASAP 2020 Plus HD88 Gas sorption analyzer, and the pore size was measured by the Barrett Joyner Halenda (BJH) methods.

3. Electro-catalytic measurements.

The electrochemical performance were conducted on a CHI 660E workstation in a standard three-electrode system. The reference electrode was saturated calomel electrode (SCE), the counter electrode was Pt wire, and the as-prepared modified electrode was used as working electrode, respectively. Specifically, 4.0 mg of Fe-N-C catalyst was dispersed by sonication in 2.0 mL ethanol consisting of 50 μL Nafion (5wt%, Dupont). The H_2O_2 yield was measured using rotating ring-disk electrode (RRDE) by a rotation speed controller (Pine Instruments) to determine the selectivity toward four-electron ORR process. The linear sweep voltammetry (LSV) curves at different speeds were recorded by gradually increased the speed from 400 to 2500 rpm on a rotating disk electrode. The number of electron transfer (n) was obtained from the Koutecky-Levich (K-L) equation:

$$J^{-1}=J_k^{-1}+(0.2nFD^{2/3}v^{-1/6}C\omega^{1/2})^{-1}$$

In this equation, J and J_k represent measured current and kinetic current, respectively. F is the Faraday constant (96485F g^{-1}), D and C are diffusion coefficient and concentration of oxygen, ν is the viscosity of the electrolyte (cm^2s^{-1}).

4. MFC Operation.

H-shaped MFCs were assembled from two glass bottles separated with a proton exchange membrane. *Shewanella oneidensis* MR-1 cells were cultivated in sterile LB broth for 24 hours at 37 °C and injected into anode chamber of MFCs. The anode chamber was composed of 5% Luria–Bertani (LB) with 18 mM lactate as the substrate, and the catholyte was O_2-saturated PBS solution. All medium were sterilized and replaced by fresh solution every 24 hours. The carbon paper (1.0 cm *1.0 cm) were used as the anode and cathode electrodes, and connected with an external load of 1000 Ω. The voltage retention and power density curves were recorded about 24 hours after inoculation.

5. DFT calculations

All the geometry relaxations and electronic property calculations within density functional theory (DFT) were performed by using Quantum Espresso.[1] The Perdew-Burke-Ernzerhof functional within the generalized gradient approximation (PBE-GGA) was used to describe the electron exchange-correlation interaction.[2] The DFT-D3 method of Grimme was used to describe long-range Van der Waals (vdW) interactions between reaction intermediates and catalysts surface.[3] The energy cutoff for the plane-wave basis expansion and convergence threshold for energy was set to 80 Ry and 0.01 eV $Å^{-1}$, respectively. The Brillouin zone was sampled with a 3 × 3 × 1 k-point mesh, the isosurface value is set to be 0.0035 e $Bohr^{-3}$. A vacuum of at least 16 Å in the z-direction was introduced to avoid the interaction between two periodic units. The computational hydrogen electrode model is applied to calculate the ($H^+ + e^-$). The limiting-potential (U_L) calculated by $U_L = [-\min(\Delta G_1, \Delta G_2, \Delta G_3, \Delta G_4)]/e$. The ORR free energy profile can be calculated by the following equations:

(1) $O_2 + * + H_2O + e^- \rightarrow OOH* + OH^-$ ΔG_1

(2) $*OOH + e^- \rightarrow O* + OH^-$ ΔG_2

(3) $*O + H_2O + e^- \rightarrow *OH + OH^-$ ΔG_3

(4) $OH* + e^- \rightarrow OH- + *$ ΔG_4

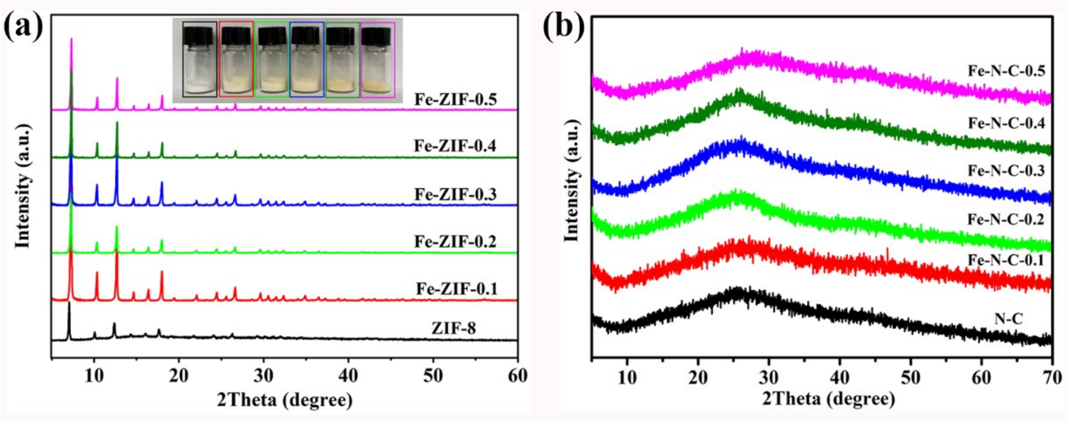

Fig. S1 XRD patterns of (a) ZIF-8 and different Fe-ZIF-X, inset is the color of ZIFs precursors; (b) N-C and different Fe-N-C-X under thermal pyrolysis at 900°C.

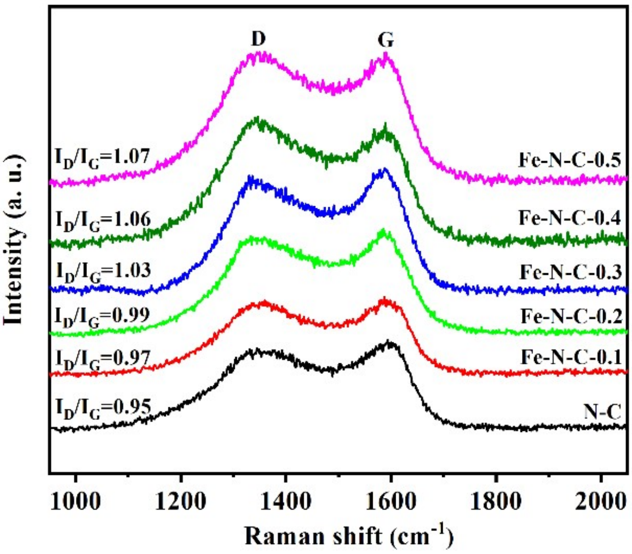

Fig. S2 Raman spectra of N-C and Fe-N-C catalysts.

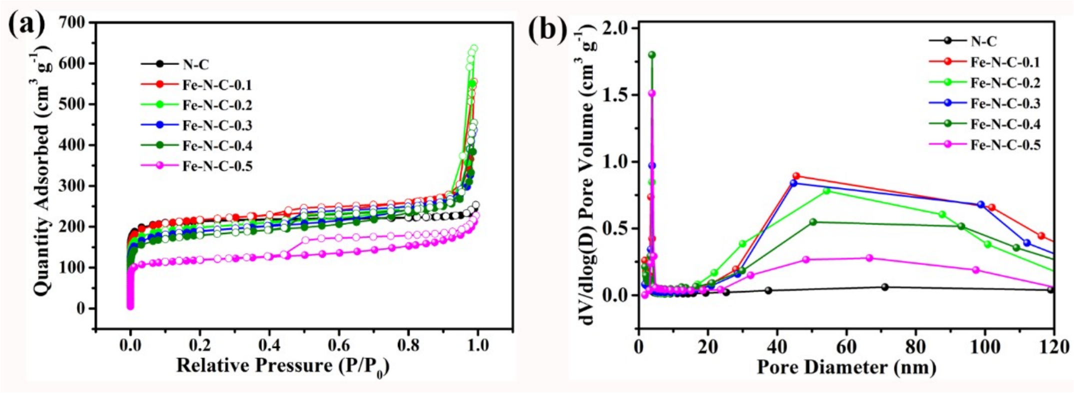

Fig. S3 (a) Nitrogen isothermal adsorption/desorption curves; (b) pore size distribution of N-C and Fe-N-C-X catalysts.

Table S1. The summarized specific surface area, and pore volumes results of N-C and Fe-N-C-X samples.

Sample	**Specific surface area** ($S_{BET,}$ cm^2 g^{-1})	**Pore volume** (cm^3 g^{-1})
N-C	505.7	0.353
Fe-N-C-0.1	666.1	0.858
Fe-N-C-0.2	610.8	0.768
Fe-N-C-0.3	587.3	0.676
Fe-N-C-0.4	558.2	0.703
Fe-N-C-0.5	399.5	0.551

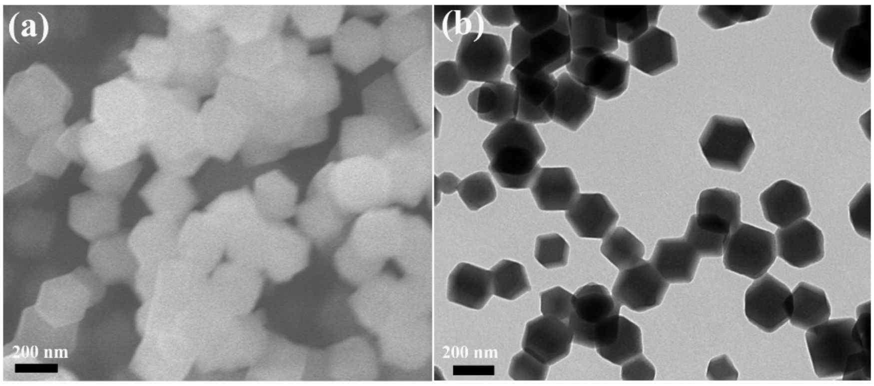

Fig. S4 (a) SEM; (b) TEM of Fe-ZIF-0.4 precursor.

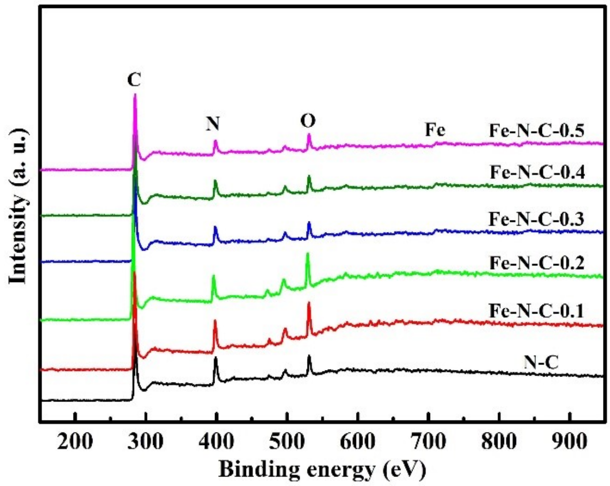

Fig. S5 XPS survey spectra of different Fe-N-C catalysts.

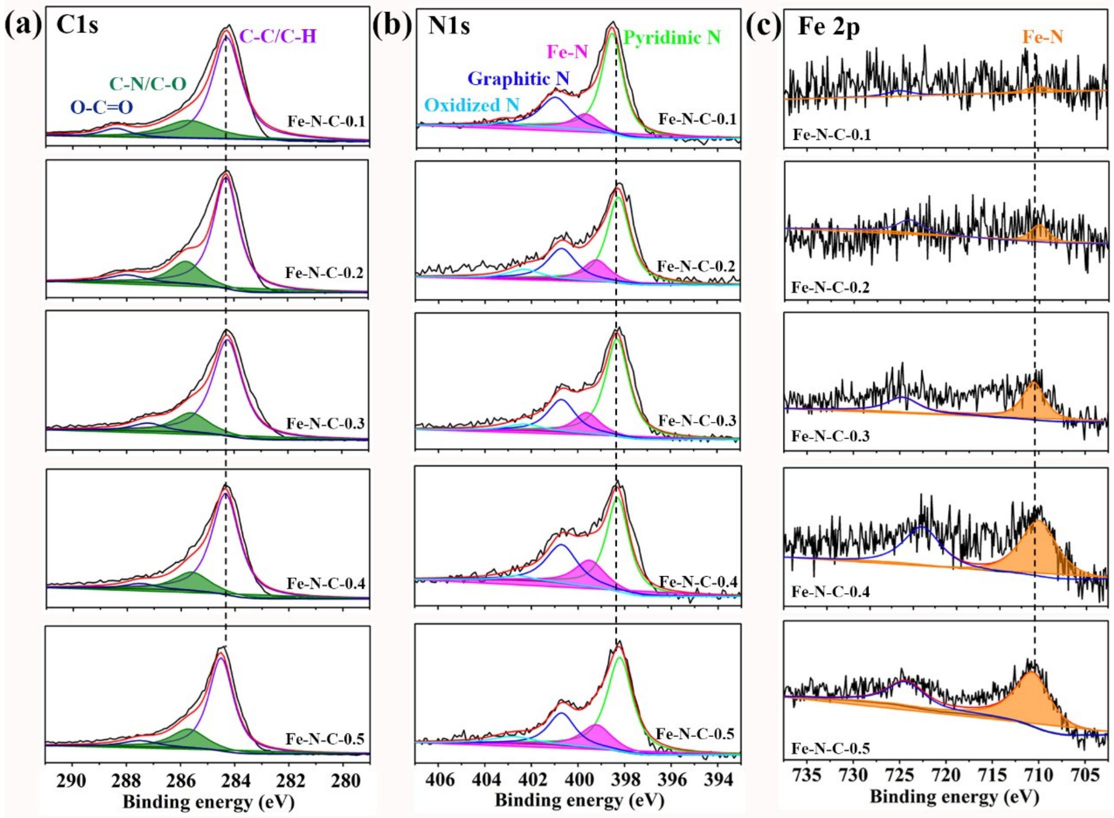

Fig. S6 Deconvoluted XPS spectra of different Fe-N-C (with increasing amount of Fe from 0.1 mM up to 0.5 mM) for (a) C1s, (b) N1s, (c) Fe2p

Table S2. Fitting results for N1s XPS spectra for different Fe-N-C-X catalysts.

Samples	Pyridinic N (at%)	Fe-N (at%)	Graphitic N (at%)	Oxidized N (at%)
Fe-N-C-0.1	2.02	0.19	1.46	0.25
Fe-N-C-0.2	1.85	0.27	1.25	0.21
Fe-N-C-0.3	1.76	0.32	1.12	0.19
Fe-N-C-0.4	1.72	0.43	1.06	0.15
Fe-N-C-0.5	1.65	0.44	1.05	0.16

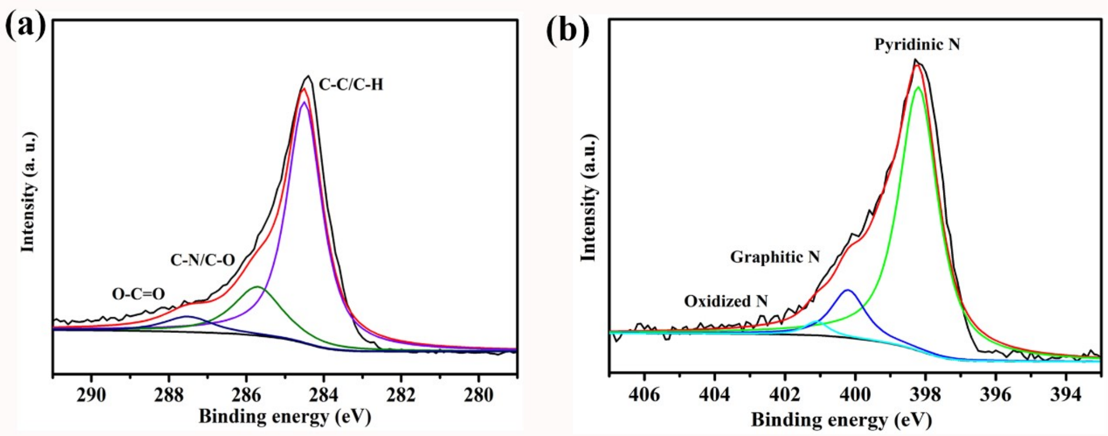

Fig. S7 Deconvoluted XPS spectra of N-C for (a) C1s, (b) N1s.

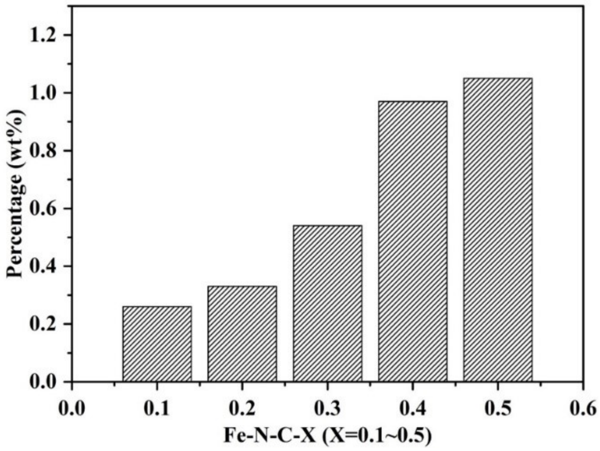

Fig. S8 ICP data for different Fe-N-C catalysts.

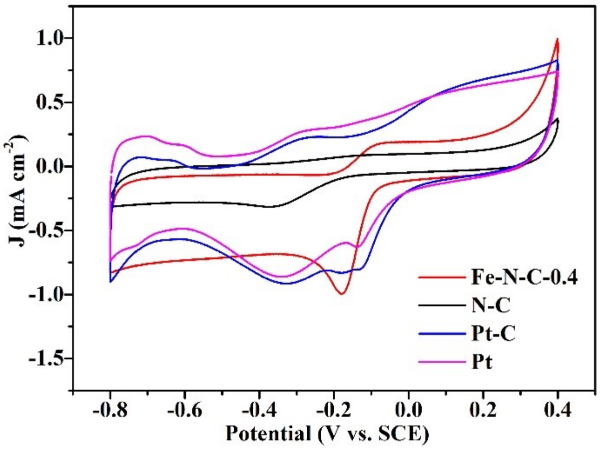

Fig. S9 CV curves of N-C, Fe-N-C-0.4, Pt/C and Pt wire electrode in O_2-saturated 50 mM PBS electrolyte.

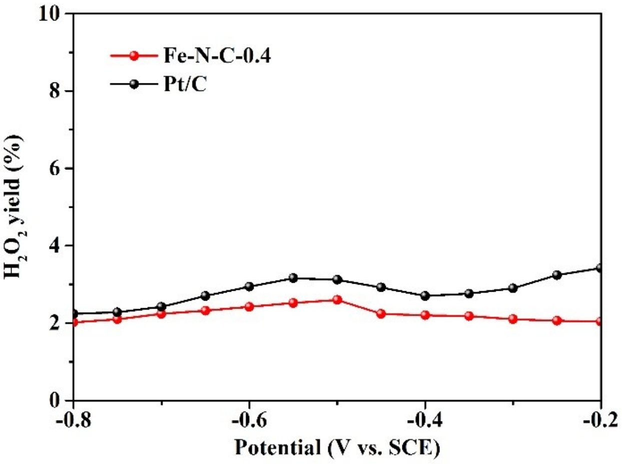

Fig. S10 H_2O_2 yield for Fe-N-C-0.4 and Pt/C.

Table S3. Comparison of MFCs with formerly reported M-N-C catalysts.

Cathode catalysts	MFC construction	Microorganism	Maximum Power density	Ref
Co-NCNTNP	single chamber MFC	wastewater	2252 mW m^{-2}	4
CoFe@Co-NC	Single-chamber MFC	wastewater	2486 mW m^{-2}	5
Co-N/S-C	Single-chamber MFC	—	1190 mW m^{-2}	6
Co-N-C	Single-chamber MFC	*Escherichia coli* K-12	1257 mW m^{-2}	7
Co-N-C	single chamber MFC	—	1665 mW m^{-2}	8
Ni/Co-NC	single chamber MFC	*Escherichia coli* K-12	4335.6 mW m^{-2}	9
FeNC-F_3	Single-chamber MFC	sewage treatment plant	0.32 mW cm^{-2}	10
Fe/N-carbon	Double chamber MFC	50/50 vol% wastewater	165 mW m^{-2}	11
Fe-N/C	Single-chamber MFC	oil-bearing sludge	1232.9 mW m^{-2}	12
Fe-N-C	Double chamber MFC	*Shewanella oneidensis* MR-1	3323 mW m^{-2}	This study

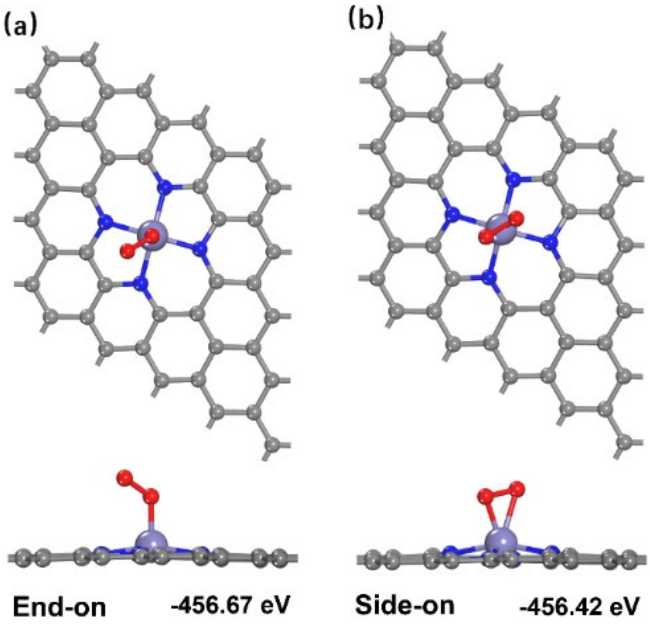

Fig. S11 The geometric structures of O_2 adsorption on Fe atom (a) end-on, (b) side-on.

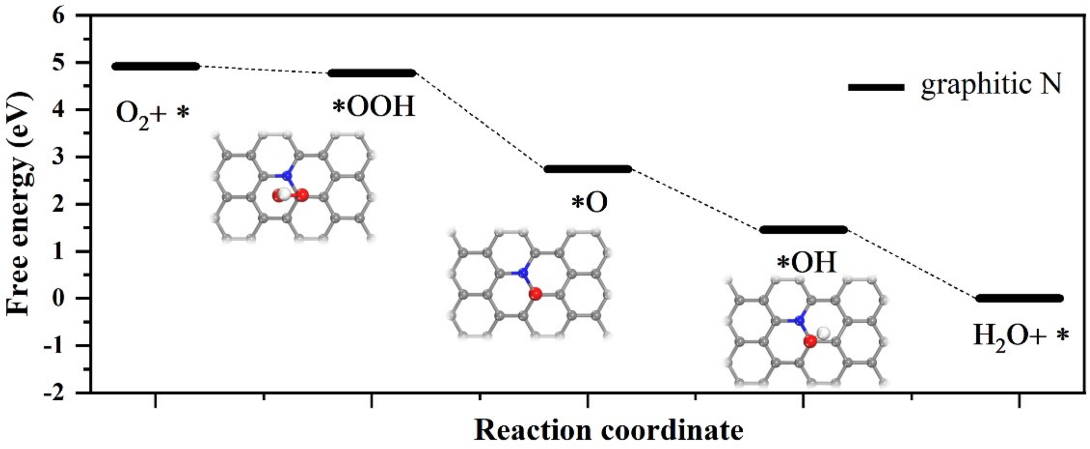

Fig. S12 The free energy diagrams for the ORR pathway on graphitic N site under the potential of U = 0 V. The limiting-potential is 1.08 V.

References

1. S. Scandolo, P. Giannozzi, Carlo Cavazzoni, Stefano de Gironcoli, P. Alfredo, B. Stefano and Z. Kristallogr, *Cond-Mat. Mtrl-Sci.*, 2005, **220**, 574-582.
2. J. P. Perdew, K. Burke and M. Ernzerhof, *Phys. Rev. Lett.,*1996, 77, 3865–3868.
3. S. Grimme, S. Ehrlich and L. Goerigk, *J. Comput. Chem.,* 2011, **32,** 1456–1465.
4. S. Zhang, W. Su, X. Wang, K. Li and Y. Li, *Biosens. Bioelectron.*, 2019, **127**, 181-187
5. X. Zhang, B. Liang, Z. Lin, M. Zhong, K. Li, H. Wang and C. Lv, *J. Power. Sources*, 2022, **520**, 230799.
6. Z. Liu, D. Wang, X. Kou, X. Dong, X. Chi, H. Ma and G. Wang, *J. Power. Sources*, 2022, **521**, 230944.
7. N. Chen, Z. Meng, R. Wang, S. Cai, W. Guo and H. Tang, *Sci. China Mater.* 2021, **64**, 2926–2937
8. S. You, X. Gong, W. Wang, D. Qi, X. Wang, X. Chen and N. Ren, *Adv. Energy Mater.* 2016, **6**, 1501497
9. H. Tang, S. Cai, S. Xie, Z. Wang, Y. Tong, M. Pan and X. Lu, *Adv. Sci.* 2016, **3**, 1500265
10. C. Shao, L. Wu, Y. Wang, K. Qu, H. Chu, L. Sun, J. Ye, B. Li and X. Wang, *Chem. Eng. J.* 2022, **429**, 132307.
11. A. Iannaci, S. Ingle, C. Dominguez, M. Longhi, O. M. Conanec, S. A.-Girard, F. Barriere, P. E. Colavita, *Bioelectrochemistry*, 2021, **142**, 107937.
12. X. Luo, W. Han, W. Du, Z. Huang, Y. Jiang and Y. Zhang, *J. Power. Sources*, 2020, **469**, 228184.